Synthesis and Characterization of *In Situ* Sodium-Activated and Organomodified Bentonite Clay/Styrene–Butadiene Rubber Nanocomposites by a Latex Blending Technique

S. Chakraborty,[1] R. Sengupta,[1] S. Dasgupta,[1] R. Mukhopadhyay,[1] S. Bandyopadhyay,[2] Mangala Joshi,[3] Suresh C. Ameta[4]

[1]*Hari Shankar Singhania Elastomer and Tyre Research Institute, Jaykaygram, P.O. Tyre Factory, Rajsamand 313 342, Rajasthan, India*
[2]*R&D Centre, J. K. Tyre, Jaykaygram, P.O. Tyre Factory, Rajsamand 313 342, Rajasthan, India*
[3]*Department of Textile Technology, Indian Institute of Technology, Delhi 110016, India*
[4]*Department of Chemistry, Mohanlal Sukhadia University, Udaipur 313 001, Rajasthan, India*

Received 13 November 2008; accepted 27 January 2009
DOI 10.1002/app.30146
Published online 2 April 2009 in Wiley InterScience (www.interscience.wiley.com).

ABSTRACT: In this article, we describe a method used to prepare an *in situ* sodium-activated, organomodified bentonite clay/styrene–butadiene rubber nanocomposite master batch via a latex blending technique. The clay master batch was used for compound formulation. Octadecyl amine was used as an organic intercalate. The clay was purchased from local suppliers and was very cheap. Sodium chloride was used for *in situ* activation of the clay. The wide-angle X-ray diffraction data indicated that the *in situ* sodium activation helped to increase the intergallery distance from 1.28 to 1.88 nm. A transmission electron micrograph indicated intercalation and partial exfoliation. The thermal properties were relatively better in the case of the sodium-activated, organomodified bentonite-clay-containing compound. A substantial improvement in physical properties such as the modulus, tensile strength, tear strength, and elongation at break was observed in the case of the *in situ* sodium-activated compound. A cation-exchange capacity equivalent (of the clay) of 1.5 times the octadecyl amine was the optimum dose for the modification. © 2009 Wiley Periodicals, Inc. J Appl Polym Sci 113: 1316–1329, 2009

Key words: nanocomposites; rubber; clay; organoclay

INTRODUCTION

The words *nanocomposites*, *nanomaterials*, and *nanofillers* are fairly recent in the polymer field, but such materials have been in use from the beginning of the last century. For example, carbon black has been used as a reinforcing filler in rubbers and in the polymer field since 1904. About 5 million metric tons of carbon black is globally consumed each year.[1] However, its polluting nature, the ubiquitous black color of the compounded rubber material, and its dependence on petroleum feedstock (for synthesis) has caused researchers to look for other white reinforcing agents. Silica is one of the major nonblack fillers in the rubber industry.[2] However, silica requires a special coupling agent to act as a reinforcing filler.[3] Although it is nonblack, clay is not used as a reinforcing filler in the rubber industry because of its big particle size and low surface activity. For a filler to behave as a good reinforcing agent, the three main factors are particle size, structure, and surface characteristics. It was only recently that researchers succeeded in intercalating polymers into the clay layers and, thereby, preparing polymer–clay nanocomposites that exhibited not only outstanding mechanical properties but also very good barrier and thermal properties. Polymer–clay nanocomposites can be prepared by solution blending, direct intercalation, the sol/gel technique, *in situ* polymerization, or latex blending.[4–15]

Most rubbers are available in the form of latex, which is nothing but an aqueous dispersion of rubber particles in the submicrometer–micrometer range (the particle size distribution depends on the manufacturing conditions). The layered silicates are easily dispersed in water as water acts as a swelling agent because of the hydration of the intergallery cations, usually Na^+ or K^+. The water-swelling capability of natural clays are not the same but depend on the type of clay and its cation-exchange capacity (CEC),[16] and hence, the mixing of the latex with the layered silicates (having a high CEC) followed by coprecipitation (coagulation) is a promising route for the production of rubber nanocomposites.[17] Varghese and Karger-Kocsis[18] prepared natural rubber

Correspondence to: S. Bandyopadhyay (sbanerjee@ktp.jkmail.com).

(NR) based nanocomposites with 10 wt % natural (sodium bentonite) and synthetic (sodium fluorohectorite) layered silicates by the latex compounding method. Wang et al.[19] prepared NR/montmorillonite and chloroprene rubber/montmorillonite clay nanocomposites by co-coagulating the rubber latex and the aqueous clay suspension. Potential application areas suggested by Wang et al.[19] for these nanocomposites were as inner tubes, inner liners, and dumpers. Stephen et al.[20] studied the impact of layered silicates such as sodium bentonite and sodium fluorohectorite on the rheological behavior of NR, carboxylated styrene–butadiene rubber (SBR) latices, and their blends with special reference to shear rate, temperature, and filler loading. Zhang et al.[21] prepared clay (natural clay fractionated from bentonite)/SBR nanocomposites by mixing SBR latex with a clay/water dispersion and coagulating the mixture. Wang et al.[22] compared the mechanical properties of clay (fractionated bentonite)/SBR nanocomposites prepared by solution and latex blending techniques and found that, at equivalent clay loadings, the nanocomposites prepared by the latex route were better than those prepared by the solution blending technique. Jia et al.[23] combined the *in situ* organic modification of montmorillonite and the latex compounding method to prepare high-performance SBR/montmorillonite nanocomposites by improving the interfacial interaction between the nanodispersed layered clay and SBR.

U.S. Patent 144401 (2003)[24] refers to the preparation of clay/rubber nanocomposites by the latex route, and such materials have been suggested for use in tire components such as tire tread, sidewalls, and/or inner liners. Another U.S. patent (065266, 2005)[25] reports the preparation of nanocomposites comprised of water sellable clay particles in aqueous emulsions such as anionic SBR or NR containing a novel amine to aid in the intercalation and partial exfoliation of the clay particles. The applications of such rubber nanocomposites are contemplated, for example, as aircraft tire tread, where a significant replacement of carbon black reinforcement is desired to reduce heat buildup for tire durability and to reduce tire weight for fuel economy.

Most of the work involves the use of sodium-activated montmorillonite clay. The sodium activation of naturally occurring montmorillonite clay involves a number of steps, which increase its cost as a starting material.[26] Moreover, the organomodification of the sodium-activated montmorillonite clay is time-consuming and further increases the cost of the montmorillonite clay. In this study, we used locally available bentonite clay, which is also known as naturally occurring montmorillonite. *In situ* sodium activation, organomodification, and SBR latex blending to prepare the nanoclay master batch was carried out in a single step. The dried clay master batch was used for compound formulation.

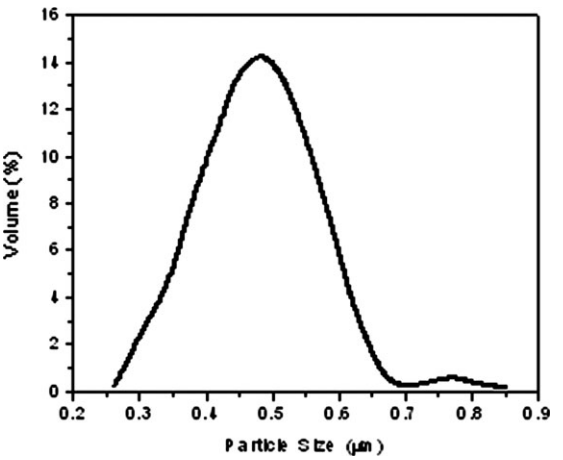

Figure 1 Particle size distribution of Encord 205.

Various researchers have shown that, with a change in the organo-amine structure, the interlayer spacing of clay changes.[27,28] As a result, the physical properties of the nanocomposite also change. It has been also reported that, when one considers a straight-chain organo-amine, the best result is achieved with octadecyl amine (ODA).[29] Thus, in this study, we used ODA as the organic intercalate.

EXPERIMENTAL

Materials

The SBR latex (Encord 205) with 25% bound styrene and 40% solid content was supplied by M/S Jubilant Organosys (Borada, India). The particle size distribution of the latex is shown in Figure 1. The Mooney viscosity (ML [1+4] at 100°C) of the coagulated SBR latex was 51. In addition to the SBR latex, SBR 1502 (emulsion-grade) from BST Elastomers [Bangkok, Thailand; bound styrene = 24%, Mooney viscosity = 50 (ML [1 + 4] at 100°C), volatile matter = 0.02%, specific gravity = 0.94] was also used in the compound formulations. Unpublished work from our laboratory indicated that the gum properties of both of these SBRs were similar, and thus, SBR 1502 was used for dose adjustment during compound formulation, as reported later. The clay used in this study was unfractionated bentonite clay available locally in Rajasthan, India. The physical and chemical characteristics of this clay are summarized in Table I, and the particle size distribution of the clay is shown in Figure 2.

The rubber compounding ingredients used in this study were commercial grade, namely, zinc oxide (ZnO), stearic acid, sulfur, and *N*-*t*-butylbenzothiazole-2-sulfenamide (TBBS). Laboratory-grade sodium chloride was procured from S.D. Fine Chemical

TABLE I
Typical Physical and Chemical Characteristics of Unfractionated Bentonite Clay

Parameter	Average value[a]
Moisture at 105°C from an IR moisture balance	10.14
pH at 25°C for a 5% aqueous solution	9.04
Nitrogen surface area (m^2/g)	76.60
Specific gravity at 26°C	2.18
325-mesh (45-μm) sieve residue (%)	<0.50
CEC (mequiv/100 g of sample)	59.0
Concentration from EDS (wt %)	
Sodium	0.88
Calcium	0.29
Aluminum	8.33
Silicon	14.84
Potassium	0.16
Magnesium	0.36
Iron	4.78
Titanium	0.89
Carbon	3.31
Oxygen	66.17

[a] Based on five individual measurements.

(Boroda, India). ODA was purchased from Merck (Mumbai, India).

Synthesis of the *in situ* modified bentonite clay nanocomposite master batch

About 10 g of the unfractionated pristine bentonite clay was dispersed in 500 mL of distilled water with a Remi, India, stirrer for 1 h at 2000–3000 rpm. The temperature was maintained around 80°C. Next, sodium chloride (10% with respect to the clay) was added to the hot clay slurry. The slurry was further stirred for 4 h at 2000–3000 rpm and 80°C. A required amount of ODA (ca. three equivalent times the CEC of the clay) was stirred with an equivalent amount of hydrochloric acid in distilled water at 80°C. The amine solution became colorless after some time. The amine solution was then added to the clay slurry, and stirring was continued for another 2 h at 80°C and 2000–3000 rpm. Diluted SBR latex (20% total solid) was then added to the aqueous slurry. The amount of latex was adjusted to make 20 parts of clay in 100 parts of rubber (i.e., 20 phr weight parts of bentonite clay per hundred weight parts of rubber) clay loading on a dry basis. The pH of the solution was adjusted to around 3–4. The solid content of the slurry was finally maintained around 20–25%. The mixture was further stirred for another 1 h. The resultant solution was coagulated during stirring. The mass was washed several times with tap water and dried at 70°C in a hot-air oven.

The same technique was followed to prepare the batches without the addition of the sodium chloride to verify the role of sodium chloride in the *in situ* sodium modification.

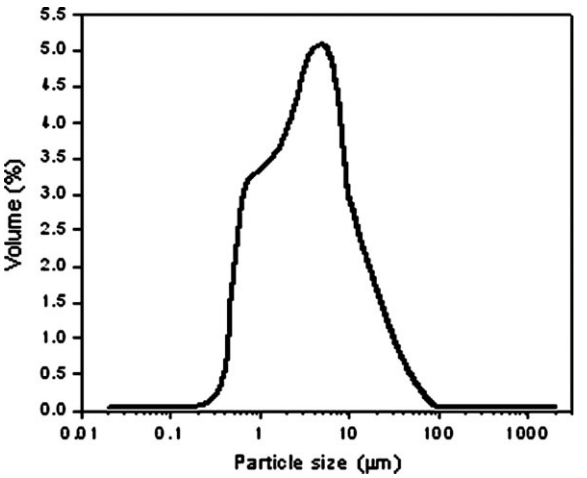

Figure 2 Particle size distribution of unfractionated bentonite clay.

The amount of amine required for the clay modification was determined by the preparation of different batches with various doses of amine, with the clay loading kept constant. The amine content was varied with respect to the CEC equivalent of the clay (0.5, 1.0, 1.5, and 2.0). The optimum doses of amine were determined from the tensile and tear properties of the different batches.

Compound mixing

The mixing was done in a single stage in a Brabender plasticorder model PL 2000-3 (M/s Brabender, Duisburg, Germany), which had a chamber volume of 80 cm^3, cam rotors, a ram pressure weight of 5 kg, and a batch weight of 70 g.

Single-stage mixing was carried out for 10 min with a 60-rpm rotor speed at 70°C. Initially, a 1-min mastication time was allowed for the rubber. Then, the clay or clay master batch was added and mixed for 6 min. Then, the other ingredients were added, and the batch was dumped after 3 min. The mixed

TABLE II
Formulations of the Compounds With and Without *In Situ* Sodium Activation

Material	A1	A2	A3	B
SBR 1502	100	100	100	100
ZnO	3	3	3	3
Stearic acid	1	1	1	1
TBBS	1	1	1	1
Sulfur	1.75	1.75	1.75	1.75
Bentonite clay	—	—	—	5
Clay from the master batch	5	—	—	—
Clay from the *in situ* organomodified master batch	—	5	—	—
Clay from the *in situ* sodium-activated, organomodified master batch	—	—	5	—

TABLE III
Formulations of the Compounds with ODA Dose Variation with Respect to the CEC Equivalent of the Clay

Material	$A3_{0.5CEC}$	$A3_{1.0CEC}$	$A3_{1.5CEC}$	$A3_{2.0CEC}$
SBR 1502	100	100	100	100
ZnO	3	3	3	3
Stearic acid	1	1	1	1
TBBS	1	1	1	1
Sulfur	1.75	1.75	1.75	1.75
Clay from the *in situ* sodium-activated, organomodified master batch	5	5	5	5

$A3_{XCEC}$ represents compound A3 to which bentonite clay was added from an *in situ* sodium-activated master batch, and the amount of ODA added during the preparation of the master batch was *X* equivalents of the CEC of clay. The SBR dose was adjusted by the addition of SBR 1502 from outside during mixing.

batches were further milled on a laboratory two-roll mill from M/s Santosh Industries (Mumbai, India). The respective compound formulations are shown in Tables II and III.

The SBR dose was adjusted by the addition of SBR 1502 from outside during mixing. The amount of ODA during *in situ* modification was deliberately kept at three equivalent times that of the CEC equivalent of the clay.

Characterization of the SBR/bentonite clay nanocomposites

The Fourier transform infrared (FTIR) spectra of the samples in the form of thin films ($\sim$ 100 μm thick, compounds A1 and A3) and of the powders (bentonite clay and ODA) were acquired with a Perkin-Elmer System 2000 FTIR spectrometer (Norwalk, CT) with a scan range of 400–4000 cm^{-1} at a resolution of 4 cm^{-1}. The spectra are represented in Figures 3 and 4.

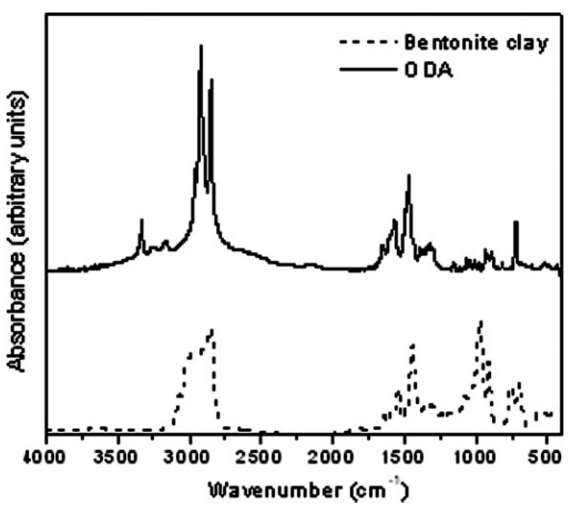

Figure 3 FTIR spectra of bentonite clay and ODA.

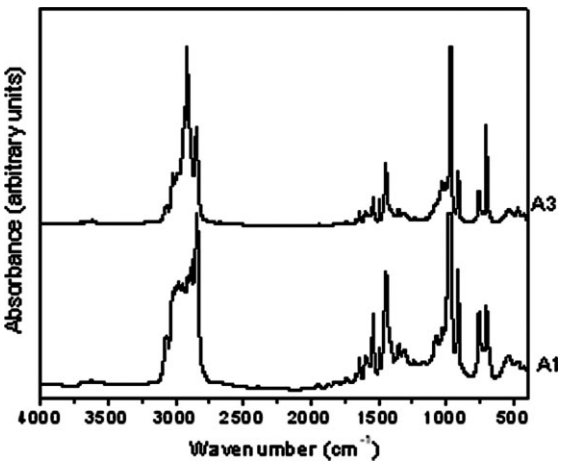

Figure 4 FTIR spectra of compounds A1 and A3.

Wide-angle X-ray diffraction (WAXD) measurements were carried out in a Philips 1710 X-ray diffractometer (Mahwah, NJ) with a scan rate of 0.5°/min with Cu Kα target at 40 kV and 25 mA (wavelength = 0.154 nm) with a 2θ scan range from 2 to 10°. The X-ray diffractograms are represented in Figures 5 and 6. The peak position and the corresponding spacing of the d_{001} plane are reported in Table IV.

For transmission electron microscopy (TEM) measurements, 100-nm sections were microtomed at −120°C with an Ultracut E ultramicrotome (Reichert and Jung) with a diamond knife. Measurements were carried out with a Philips CM200 transmission electron (Eindhoven, The Netherlands) microscope at an acceleration voltage of 120 kV. The TEM micrograph of compound A3 is given in Figure 7(A).

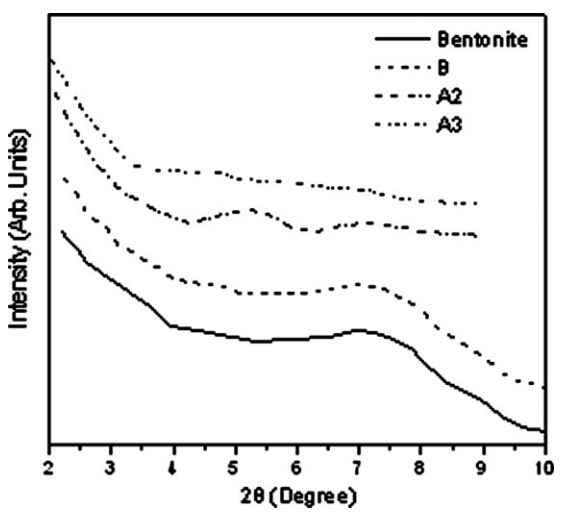

Figure 5 X-ray diffractograms of compounds B, A2, and A3 and bentonite clay.

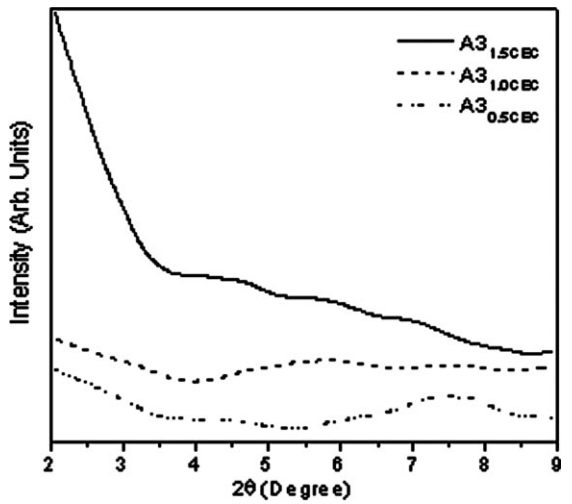

Figure 6 X-ray diffractograms of compounds $A3_{1.5CEC}$, $A3_{1.0CEC}$, and $A3_{0.5CEC}$.

Scanning electron microscopy (SEM) was performed with a Jeol JSM 6390LV (Tokyo, Japan) instrument in low-vacuum mode without any metal coating. An energy-dispersive X-ray spectrophotometry (EDS) study was carried out with the help of a Quantax 200 instrument with an X-Flash liquid nitrogen free detector from Bruker (Berlin, Germany) for the elemental mapping of the samples. The silicon and aluminum mapping of the samples are reported in Figures 8 and 9.

We determined the thermal stability of the cured samples by carrying out thermogravimetric analysis (TGA) using a Pyris-1 thermogravimetric analyzer from PerkinElmer (Shelton, CT) from the TGA study. For each sample, three tests were carried out with the same heating rate, and the temperatures were reproducible to ±3.0°C. Initially, the sample was heated under a nitrogen atmosphere up to 600°C, and then, the gas was changed to oxygen, and the heating was continued up to 800°C. The heating rate was 40°C/min. The TGA and differential thermogravimetry (DTG) thermograms are shown in Figures 10 and 11, respectively. The decomposition data are represented in Table V.

TABLE IV
Peak Position (2θ) and Corresponding Spacing of the d_{001} Plane of the Compounds

Compound	2θ (°)	d_{001} (nm)
Bentonite clay	7.2	1.23
B	7.2	1.23
A2	5.3 with a second peak at 6.9	1.67
A3	Nearly flat with a hump at 4.7	1.88
$A3_{0.5CEC}$	7.2	1.23
$A3_{1.0CEC}$	5.5	1.60
$A3_{1.5CEC}$	Nearly flat with a hump at 4.7	1.88

Differential scanning calorimetry (DSC) experiments were performed in dynamic mode with a Diamond differential scanning calorimeter (Perkin-

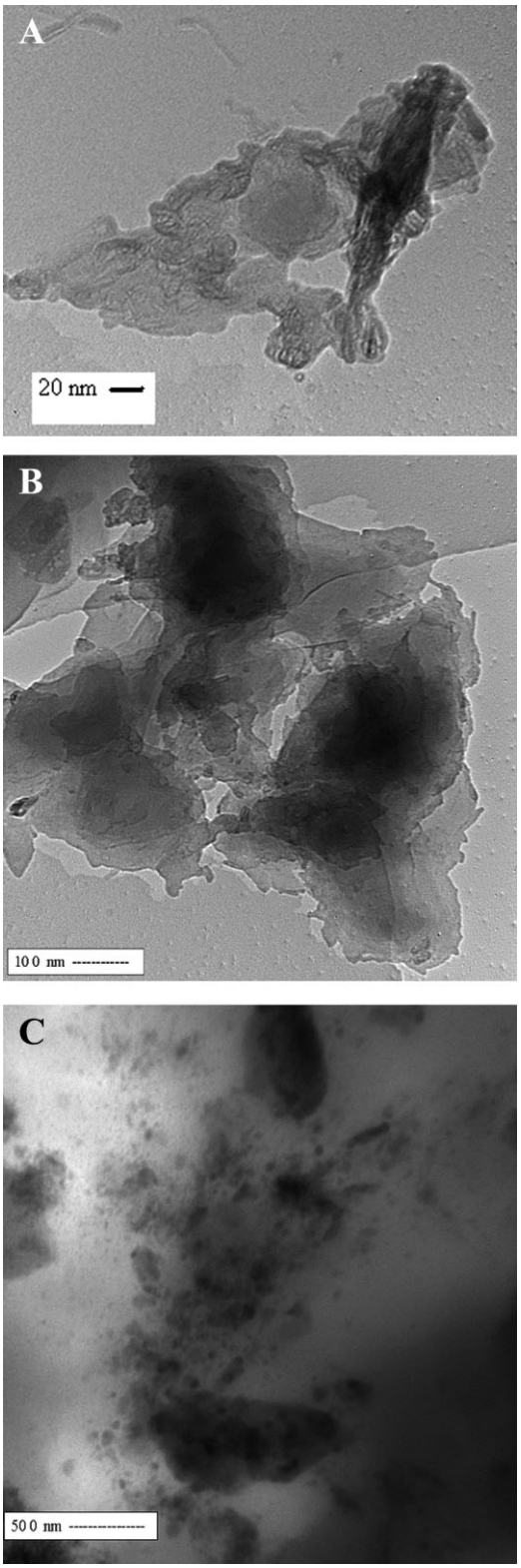

Figure 7 TEM images of (A) compound A3, (B) compound A3 with a stack of clay particles with a high aspect ratio, and (C) compound A3 showing impurity particles.

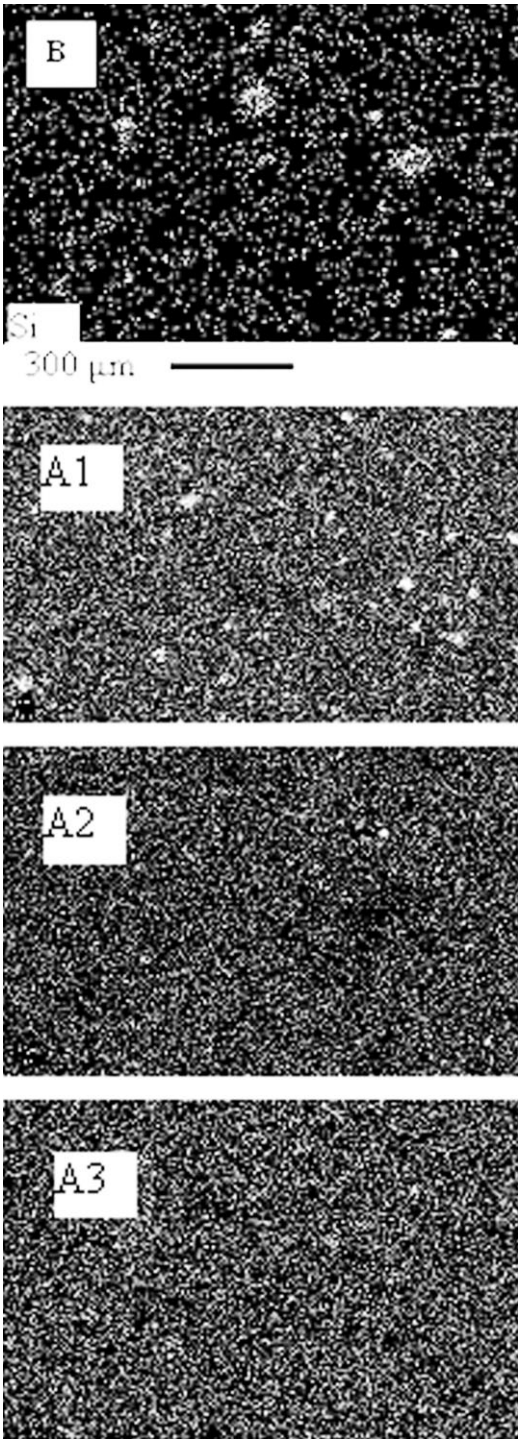

Figure 8 Si mapping of compounds B, A1, A2, and A3 by EDS.

Elmer, Norwalk, CT) to measure the glass-transition temperature (T_g). The scanning rate was 20°C/min under a nitrogen atmosphere. The DSC thermograms are shown in Figure 12, and the T_g values are reported in Table VI.

The rheometric properties were determined in a moving die rheometer (MDR 2000E) from M/s Alpha Technologies (Akron, OH) at 160°C for 30 min, with the rotor arc kept at 0.5° in accordance with ASTM D 5289. The rheometric properties are reported in Tables VII and VIII.

The curing of the tensile slabs was done with a compression molding technique in an electrically heated curing press from M/s Hind Hydraulics (New Delhi, India) at 160°C for 30 min. The tensile

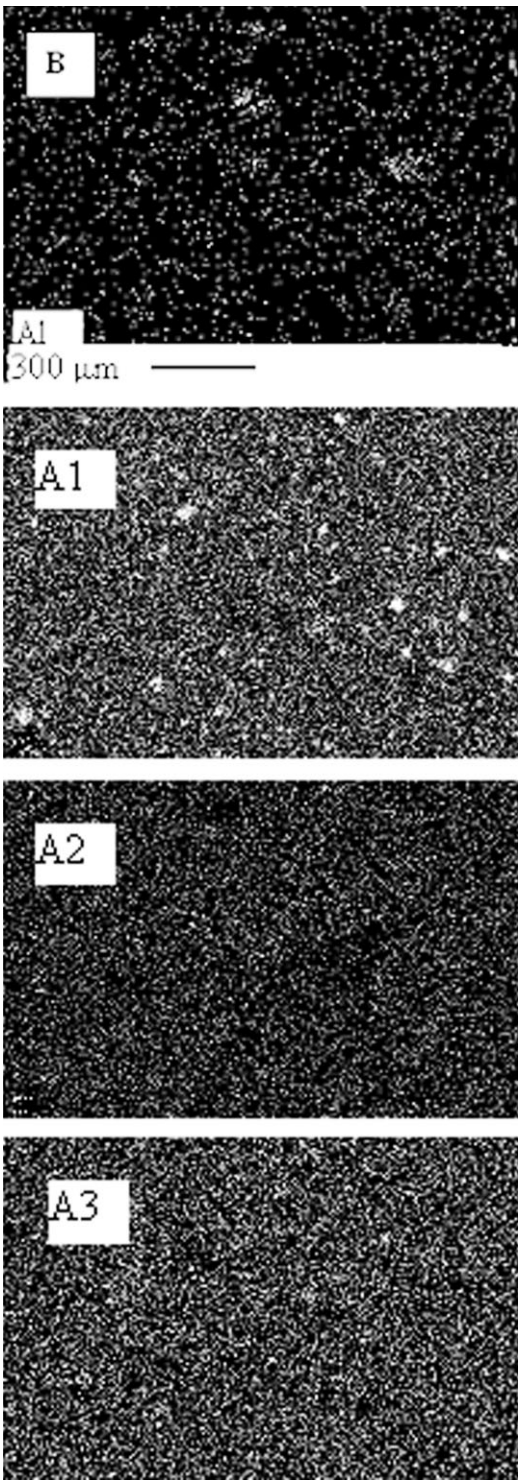

Figure 9 Al mapping of compounds B, A1, A2, and A3 by EDS.

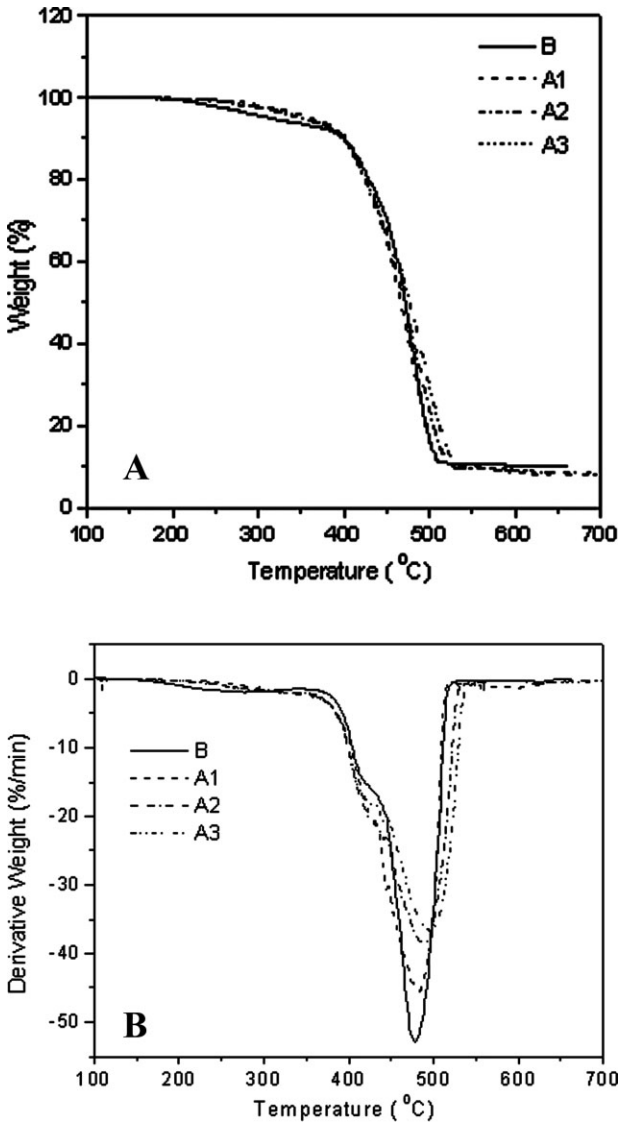

Figure 10 (A) TGA and (B) DTG thermograms of compounds B, A1, A2, and A3.

samples were died out in accordance with an ASTM D 412 type C die.

The stress–strain properties were determined with a universal testing machine (Zwick UTM 1445, M/s Zwick, Ulm, Germany) in accordance with ASTM D 412. The hardness was determined in a Shore A durometer from M/s Prolific Industries (New Delhi, India) in accordance with ASTM D 2240.

The tear properties were measured according to ASTM D 624. The Mooney viscosity was measured with a MV2000E instrument from Alfa Technologies (Akron, OH) in accordance with ISO 289-1.

The cure rate index (CRI) was measured according to ASTM D 5289. The following formula was used for CRI in this study:

$$\mathrm{CRI} = \frac{100}{t_{c90} - t_{s2}} \tag{1}$$

where t_{c90} is the time to 90% cure and t_{s2} is the scorch time.

The swelling index of the cured samples was measured with the following formula in accordance with ASTM D 3616.

$$\text{Swelling index} = \frac{\text{Swollen weight}}{\text{Initial weight}} \tag{2}$$

The volume fraction was also measured to get an indication of apparent crosslink density. A weighed sample of cured rubber vulcanizate was immersed in a toluene solvent for 48 h at room temperature. Excess solvent was then blotted from the sample, and the swollen weight was measured. The swollen sample was dried in oven at 100°C until a constant weight was reached. The dried weight of the sample was taken after the sample was cooled in a desiccator. The volume fraction of the vulcanizate rubber (V_r)[30,31] was calculated with the following formula:

$$V_r = \frac{(D - FT)/\rho_r}{(D - FT)/\rho_r + A_0/\rho_s} \tag{3}$$

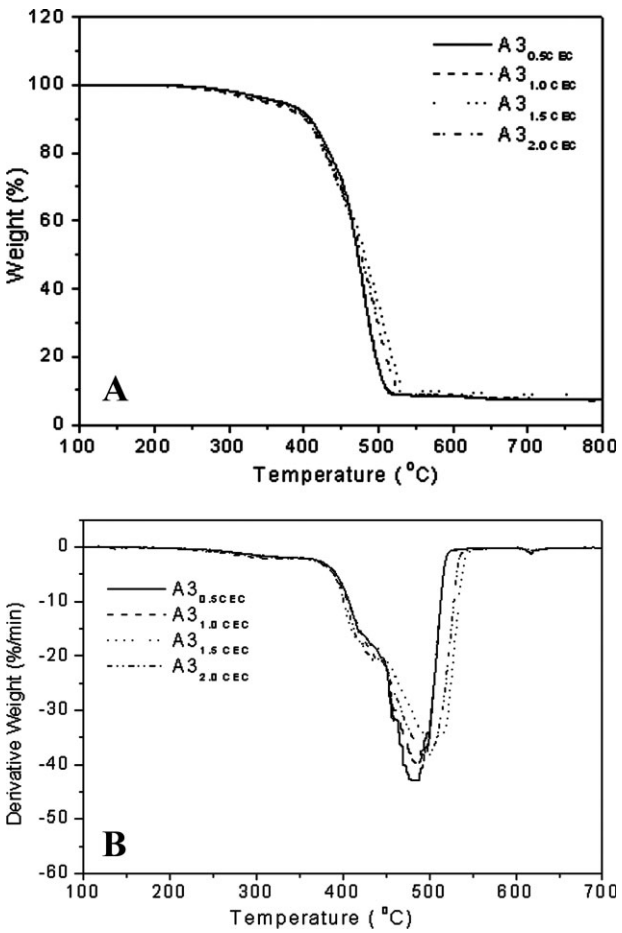

Figure 11 (A) TGA and (B) DTG thermograms of compounds $A3_{0.5CEC}$, $A3_{1.0CEC}$, $A3_{1.5CEC}$, and $A3_{2.0CEC}$.

TABLE V
Thermogravimetric Data for Various Compounds

Sample	Decomposition up to 400°C (%)	Peak decomposition temperature (°C)	Peak decomposition rate (%/min)
A1	9.6	482.6	45.7
A2	9.9	490.7	39.0
A3	8.8	496.0	36.0
B	9.6	482.0	52.8
$A3_{0.5CEC}$	8.9	480	44.5
$A3_{1.0CEC}$	9.0	484	40.0
$A3_{1.5CEC}$	8.7	501	35.0
$A3_{2.0CEC}$	8.9	496	39.0

where D is the weight of the deswollen sample, F is the weight fraction of the insoluble nonrubber ingredients, T is the original dry weight of the sample, A_0 is the weight of solvent absorbed, ρ_r is the density of the rubber (the density value was 910 kg/m^3), and

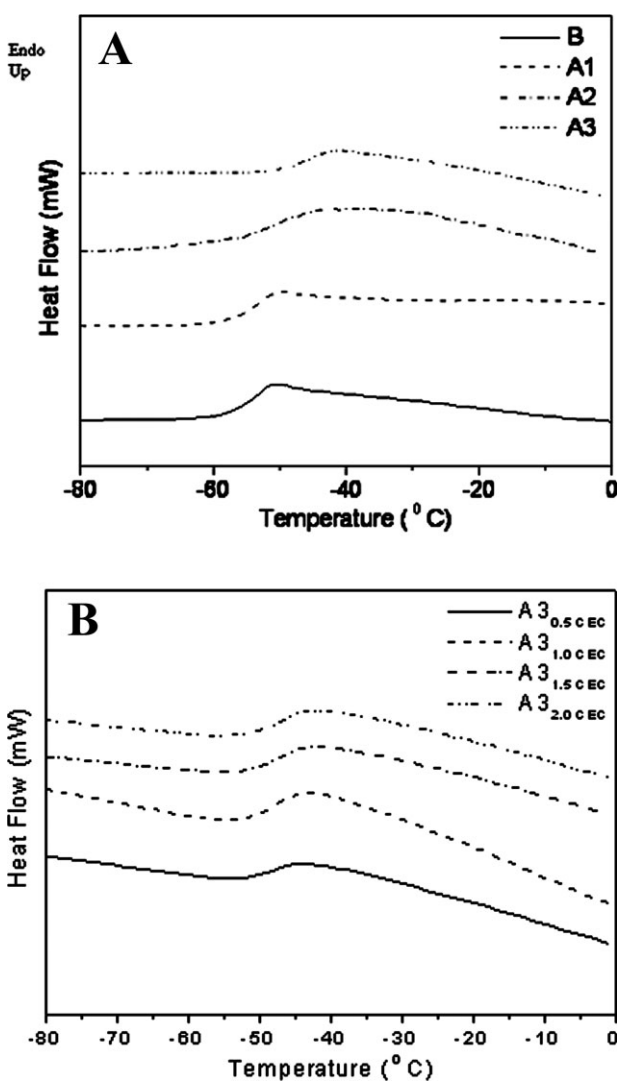

Figure 12 DSC thermograms of (A) A1, A2, A3, and B and (B) $A3_{0.5CEC}$, $A3_{1.0CEC}$, $A3_{1.5CEC}$, and $A3_{2.0CEC}$.

TABLE VI
T_g Values of Different Compounds

Compound	T_g (°C)
A1	−53.2
A2	−50.7
A3	−45.4
B	−54.5
$A3_{0.5CEC}$	−48.3
$A3_{1.0CEC}$	−47.5
$A3_{1.5CEC}$	−46.2
$A3_{2.0CEC}$	−46.0

ρ_s is the density of the solvent (the density value was 870 kg/m^3).

The bound rubber content was also measured with the following formula[32]

$$\text{Bound rubber} = \frac{(M_B - M_F - M_D)}{M_B} \times 100\% \quad (4)$$

where M_B is the weight of the uncured mix before immersion, M_F is the weight of the filler in the uncured mix, and M_D is the weight of the rubber dissolved in the solvent.

The rebound resilience and compression set of the samples were determined according to ISO 4662 and ASTM D 395, respectively.

The physical properties are summarized in Table IX.

RESULTS AND DISCUSSION

From the tentative chemical composition analysis of the bentonite clay by EDS, it was clear that the bentonite clay was impure in nature. The presence of transition metals also indicated the impurity of the clay. The atomic percentage of different metals, as reported in Table I, supported this fact. The presence of calcium and sodium indicated that the clay was a mixture of sodium and calcium montmorillonite. The CEC of this unfractionated bentonite clay was low compared to commercially available synthetic montmorillonite.[33]

The average particle size of the bentonite clay was around 3000 nm, and that of the latex particles was 500 nm.

TABLE VII
Rheometric Properties of Compounds A1, A2, A3, and B

Parameter	A1	A2	A3	B
T_{max} (dN m)	6.2	6.7	6.9	6.3
T_{min} (dN m)	1.0	0.9	0.5	1.6
$T_{max} - T_{min}$ (dN m)	5.2	5.8	6.4	4.7
t_{s2} (min)	14.1	4.3	4.6	13.3
t_{c90} (min)	27.9	14.0	12.3	24.3
CRI (min^{-1})	7.2	10.3	13.0	9.1

T_{max} = maximum torque; T_{min} = minimum torque.

TABLE VIII
Rheometric Properties of Compounds $A3_{0.5CEC}$, $A3_{1.0CEC}$, $A3_{1.5CEC}$, and $A3_{2.0CEC}$

Parameter	$A3_{0.5CEC}$	$A3_{1.0CEC}$	$A3_{1.5CEC}$	$A3_{2.0CEC}$
T_{max} (dN m)	6.2	6.4	6.7	6.6
T_{min} (dN m)	1.3	0.9	1.1	1.1
$T_{max} - T_{min}$ (dN m)	4.9	5.5	6.6	6.5
t_{s2} (min)	10.0	6.6	4.7	3.4
t_{c90} (min)	20.0	15.5	12.5	11.0
CRI (min^{-1})	10	11.2	12.8	13.5

T_{max} = maximum torque; T_{min} = minimum torque.

FTIR study

The FTIR spectra of the dry bentonite clay and ODA are represented in Figure 3. The bentonite clay showed characteristic bands at approximately 3700–3400 cm^{-1} (OH stretching of Si—OH groups), 1640 cm^{-1} (deformation vibrations of the interlayer water in the clay), and 1030 cm^{-1} (asymmetric Si—O—Si stretching).[34] The ODA showed characteristic antisymmetric and symmetric stretching frequency of the N—H bond of primary amine at approximately 3300 and 3250 cm^{-1}. N—H deformation was found at approximately 1600 cm^{-1}, and C—N stretching was found at approximately 1300 cm^{-1} (kemp). In Figure 4, the spectra of compounds A1 and A3 are nearly the same. This was because of the overlapping of the characteristic bands of ODA with those of SBR and bentonite clay. However, a very strong peak at approximately 3000 cm^{-1} indicated the presence of amine salts (hydrohalides)[35] and, thereby, provided evidence for the presence of amine in the modified batches.

Dispersion morphology of the SBR/clay nanocomposites

WAXD study

Figure 5 shows the X-ray diffraction (XRD) patterns of the bentonite clay and compounds B, A2, and A3,

TABLE IX
Physical Properties of Compounds A1, A2, A3, B, $A3_{0.5CEC}$, $A3_{1.0CEC}$, $A3_{1.5CEC}$, and $A3_{2.0CEC}$

Parameter	A1	A2	A3	B
50% modulus (MPa)	0.62	0.67	0.64	0.58
300% modulus (MPa)	2.03	2.18	2.82	1.75
Tensile strength (MPa)	3.48	4.13	7.01	2.10
Elongation at break (%)	457	529	743	361
Hardness (S)	45	46	47	45
Work to fracture (J)	1.25	1.71	3.03	0.69
Swelling index	5.72	5.31	5.20	5.94
V_r	0.140	0.146	0.150	0.136
Tear (N/mm)	17.88	23.1	22.8	12.90
Bound rubber (%)	13.0	11.3	16.2	8.2
Mooney viscosity [ML (1+4) at 100 °C]	47.2	48.0	50.1	46.7
Rebound resilience	62.0	59.0	57.5	67.8
Compression set at 105°C/24 h (%)	38	40.5	41.5	35.0

Parameter	$A3_{0.5CEC}$	$A3_{1.0CEC}$	$A3_{1.5CEC}$	$A3_{2.0CEC}$
50% modulus (MPa)	0.65	0.63	0.64	0.62
300% modulus (MPa)	2.16	2.01	2.82	1.77
Tensile strength (MPa)	5.12	5.21	7.01	6.51
Elongation at break (%)	681	711	740	737
Hardness (S)	47	48	47	47
Work to fracture (J)	3.11	3.00	3.03	2.96
Swelling index	5.80	5.30	5.21	5.23
V_r	0.132	0.153	0.160	0.160
Tear (N/mm)	21.7	21.4	22.8	21.5
Bound rubber (%)	9.0	13.0	16.5	16.0
Compression set at 105°C/24 h (%)	38.5	39.0	40.0	41.0
Rebound resilience	62.0	61.0	58.0	58.4
Mooney viscosity [ML (1+4) at 100 °C]	49.0	49.5	51.0	50.5

The tensile and tear properties of the compounds are the means of five measurements, and the rest of the properties are the averages of the two measurements.

respectively. The bentonite clay showed a characteristic diffraction peak at $2\theta \approx 7.2^\circ$, which corresponded to an intergallery distance of 1.23 nm. Compound B did not exhibit any shift in the diffraction peak, and thus, the intergallery distance in compound B remained the same as in case of the bentonite clay. We deduced that the incorporation of the clay gave rise to the formation of a conventional composite at a microscopic level, where the polymer was not intercalated into the silicate galleries. However, the harmonic peaks observed in the intensity curve for compound A2 represented higher orders of *d*-spacing between the silicate layers, and this indicated a higher degree of ordering induced in the silicate layers.[36] It indicated that the clay layers were in stacked condition and the polymer chains were diffused inside the interlayer galleries of the clays. In the case of compound A3, the XRD diffraction patterns were nearly flat with hump at 4.7°, which corresponded to a layer spacing of 1.88 nm. The intercalation of the polymer and the partial exfoliation of the clay layers led to a disordering of the layered clay structure, which caused the decrease in the XRD coherent layer scattering intensity of compound A3. Thus, the *in situ* sodium activation and organomodification helped to increase the interlayer spacing of the bentonite clay. It is important to mention here that the amine content in compounds A2 and A3 was threefold that of the CEC equivalent of the clay.

Figure 6 shows the XRD patterns of compounds $A3_{0.5CEC}$, $A3_{1.0CEC}$, and $A3_{1.5CEC}$. In compound $A3_{0.5CEC}$, the interlayer spacing was 1.2 nm compared to 1.6 and 1.9 nm in compounds $A3_{1.0CEC}$ and $A3_{1.5CEC}$. Thus, for this clay, 1.5 times the CEC equivalent (of the clay) of the amine was taken as the optimum level for the treatment of the clay. This was also confirmed from the physical property testing.

The findings are summarized in Table IV.

TEM study

The TEM photomicrograph of compound A3 shown in Figure 7(A) clearly points out the exfoliated and intercalated nature of the SBR bentonite clay nanocomposite. Totally exfoliated clay particles are shown at the upper left corner of the TEM micrograph, whereas the intercalated clay particles are in the middle of the micrograph. Figure 7(B) indicates the stack of clay particles with a high aspect ratio. Figure 7(C) shows the large impure particles.

SEM–EDS study

Figure 8 compares the Si mapping of compounds B, A1, A2, and A3, respectively. It is evident that there was significant aggregation of the bentonite clay in B and A1. However, the Si signals from A3 proved that the bentonite clay was homogeneously distributed in the SBR matrix. Slight aggregation was observed in A2 as there was no sodium activation. Similarly, the Al mapping of B, A1, A2, and A3 shown in Figure 9 corroborated the Si mapping findings. The magnification of the pictures were low enough (300 μm) and, thus, could be taken as a representative picture for the whole sample.

Effect of clay on the thermal behavior

TGA study

The TGA and DTG curves of compounds A1, A2, A3, B, $A3_{0.5CEC}$, $A3_{1.0CEC}$, $A3_{1.5CEC}$, and $A3_{2.0CEC}$ are compared in Figures 10 and 11; with the decomposition up to 400°C, the peak decomposition temperatures and the corresponding peak decomposition rates for the compounds are tabulated in Table V. The decomposition amount up to 400°C (onset decomposition) was around 9% in the case of compound A3 compared to that of approximately 10% for compounds A1, A2, and B. The peak decomposition temperature followed the trend A3 > A2 > A1 > B, and the exact reverse trend was followed for the peak decomposition rate. Compound B contained ordinary bentonite clay and thus formed a conventional composite with a very low degree of dispersion with large aggregates. In compound A1, the clay was added from the SBR latex/bentonite clay master batch. This helped the clay to disperse properly compared to compound B. In case of compound A2, the clay was added from the master batch in which ODA (amine hydrochloride) was added during the master batch preparation stage but no sodium chloride was added. Compound A3 contained the master batch in which the sodium chloride was added before the addition of the amine hydrochloride. Thus, the *in situ* sodium activation helped the compound to achieve a higher thermal resistance because of relatively better exfoliation and/or intercalation of the SBR into the clay gallery. The better thermal stability was attributed to the carbonaceous char formed and the structure of the clay minerals. The multiplayer clay structure acted as an excellent insulator and barrier for mass transfer.

Optimum thermal resistance was found in case of compound $A3_{1.5CEC}$. In case of compound $A3_{1.5CEC}$, better dispersion was expected because of the high level of nanoscopic dispersion of the clay in the rubber matrix, as supported by XRD data.

DSC study

Dynamic DSC scans for the samples are shown in Figure 12(A,B), and the values are tabulated in Table

VI. T_g of compound B was observed at approximately −55°C, whereas A1, A2, and A3 exhibited T_g's at approximately −53, −51, and −45°C, respectively. These peak shifts can be explained on the basis of restricted mobility of the SBR chains within the bentonite layers, which thereby proved the intercalated/exfoliated nature of the SBR/ODA modified bentonite clay nanocomposites.[34] Thus, in case of compound A3, effective intercalation and/or exfoliation of the of the clay increased the T_g.

T_g of compound $A3_{0.5CEC}$ was observed at −48.3°C, whereas $A3_{1.0CEC}$, $A3_{1.5CEC}$, and $A3_{2.0CEC}$ exhibited T_g's at −47.5, −46.2, and −46.0°C, respectively. T_g of compound $A3_{1.5CEC}$ was higher compared to $A3_{0.5CEC}$ and $A3_{1.0CEC}$. This indicated that the optimum amine required for the treatment of the clay was 1.5 times that of the CEC equivalent of the clay.

Cure kinetics

The cure properties of the compounds are compiled in Tables VII and VIII, respectively. The extent of curing [given by the torque change values (Maximum torque − Minimum torque)] was highest in compound A3 followed by compound A2. This may be explained by the effective intercalation of the SBR chains into the galleries of the bentonite clay, which resulted in a higher rubber-to-filler interaction. Compound A3 exhibited a high CRI value followed by A2, A1, and B. It seemed that the organoclay acted as an effective vulcanizing agent. The ODA present within the nanosilicate layer of the clay facilitated the vulcanization reaction. In compound A3, *in situ* sodium activation increased the amount of amine within the clay nanolayers. As a result, the availability of the organo-amine was higher in compound A3 as compared to compound A2. This gave rise to the higher CRI value for compound A3.[34] Compound A1 exhibited a higher torque change (Maximum torque − Minimum torque) compared to compound B, but this value was lower in comparison to those of compounds A2 and A3. In compound A1, a better dispersion of the bentonite clay occurred because of the latex stage master batching, which resulted in a higher rubber–filler interaction compared to that in compound B. Compound B was a conversional composite with a microscale level dispersion of the bentonite clay. Compound A3 exhibited the highest torque change (Maximum torque − Minimum torque) because of the nanoscopic dispersion of the clay in the rubber matrix.

However, CRI was lower in the case of compound A1 than in compound B. The lower cure rate with respect to compound B was due to the increased interaction of the curative with the dispersed clay layers. It has been reported that fillers such as silica reduce the cure rate because of the interaction of the polar —OH groups with the accelerator molecules.[2] It was observed that t_{s2} decreased drastically whenever organo-amine was used. This was expected because amines are regarded as scorchy accelerators.[37]

The t_{s02} and t_{c90} values decreased as the amine content was increased from $A3_{0.5CEC}$ to $A3_{2.0CEC}$. It was obvious, as discussed previously. Also, the torque change (Maximum torque − Minimum torque) reached the maximum for compound $A3_{1.5CEC}$.

Tables VII and VIII indicate that, except for compounds A1 and $A3_{0.5CEC}$, all of the other compounds had a low t_{c90} value. The rheometer data indicated a flat curing, and there was practically no reversion after 30 min of curing. Thus, the curing of the tensile and tear slabs was carried out for 30 min to give same amount of heat history to all of the compounds and to observe any discoloration of the compounds due to the presence of amine. There was no discoloration of the compounds.

Physical properties

The mechanical properties, namely, the 50 and 300% moduli, tensile strength, and work to fracture, were at a maximum in compound A3. The more effective intercalation and/or exfoliation of the SBR chains in the organo-amine-modified clay were probably responsible for the increase in the tensile properties in compound A3 compared to the other compounds. Both A2 and A3 contained the same parts per hundred rubber of bentonite filler, but the sole difference between them was that bentonite was *in situ* sodium-activated in A3, and as a result, corresponding increases in the unaged 50% modulus, 300% modulus, tensile strength, elongation at break, work to break, and tear strength over compounds B, A1, and A2 were observed. The increase in the interlayer spacing in compound A3 compared to that of A1, A2, and B also supported the effective intercalation and/or exfoliation of the clay in compound A3.

The reason for the increases in the work to fracture, tear strength, and bound rubber content was the same.

The elongations at break of compounds A2 and A3 was significantly higher in comparison to those of A1 and B. It has been reported that organoclay nanocomposites show higher elasticity because of better compatibility between the organoclay and the elastomer.[10]

The hardness of the compounds remained nearly same. The lowest swelling index in the case of compound A3 was due to higher mechanical anchorage of the polymer chains in side of the clay platelet. This explanation also indirectly supported the better mechanical properties of compound A3. For the

same reason, the Mooney viscosity of compound A3 was highest followed by those in compounds A2, A1, and B.

The modulus, tensile strength, tear strength, elongation at break, and work to fracture reached maximum values in compound $A3_{1.5CEC}$. At higher amine levels, the excess amine probably acted as lubricating agent, and thus, there was no further improvement. Thus, 1.5 times amine (with respect to the CEC equivalent of the bentonite clay) was taken as the optimum level for the treatment of the clay. This was also supported by the XRD data, as there was no further increase in the interplanar distance with increasing amine content (compound A3). The hardness of the compounds remained the same, as the total filler loading was the same.

The lowest swelling index in case of compound $A3_{1.5CEC}$ was due to the higher mechanical anchorage of the polymer chains inside the clay platelet. This explanation also indirectly supported the better mechanical properties of the $A3_{1.5CEC}$ compound. Because of the same reason, the Mooney viscosity of compound $A3_{1.5CEC}$ was highest, followed by $A3_{2.0CEC}$, $A3_{1.0CEC}$, and $A3_{0.5CEC}$.

The bound rubber content was high in the case of compound $A3_{1.5CEC}$ because of the higher rubber–filler interaction generated from the intercalation of the rubber chain into the interlayer spacing of the clay.

The rebound resilience of compound A3 was lowest, followed by those of A2, A1, and B, respectively. This was due to the particle size of the filler or the surface area of the filler available for the interaction with the rubber chains.[38] In case of compound A3, sodium activation helped effective organomodification, and hence, better intercalation and or exfoliation occurred. In compounds A2 and A1, no such activation took place. In compound B, no intercalation and or exfoliation occurred, as indicated by WAXD.

A lower rebound indicated an increase in the viscous part of the compound. This directly explained the trend of the compression set for the A1, A2, A3, and B compounds.

The same trend was observed for the $A3_{0.5CEC}$, $A3_{1.0CEC}$, $A3_{1.5CEC}$, and $A3_{2.0CEC}$ compounds and could be explained in the same way.

Mechanism of *in situ* sodium activation and organomodification

The average size of the latex particle was around 500 nm, whereas the interlayer spacing of the clay particles after amine treatment was around 2 nm. Thus, it seemed that the latex particles or coil conformed rubber molecules were too big to intercalate the clay particles. During mixing of the organoclay in the internal mixer or two-roll mills, the high shearing force delaminated some of the clay plates and, thus, facilitated the intercalation of the rubber molecules into the clay. In exfoliation, the complete delamination of the clay particles occurred. If we consider the nonmodified and organomodified clay, the later one generated favorable thermodynamic conditions for the rubber molecules to intercalate or exfoliate the clay particles.[39]

It has been reported[40] that sodium montmorillonite swells easily in water, as water acts as a swelling agent because of the hydration of the intergallery cations. The rate of swelling is faster in the presence of less hydrated monovalent ions, such as Na^+, Rb^+, K^+, and Cs^+. However, multivalent ions, such as Ca^{++}, Mg^{++}, and Fe^{+3}, reduce the rate of swelling. Calcium montmorillonite does not swell as well as sodium/potassium montmorillonite.

The montmorillonite can undergo a cation exchange reaction[41] in an aqueous medium. When a sodium chloride solution is added to the aqueous slurry of the bentonite clay, the montmorillonite fraction of the clay can undergo the following type of reaction:

$$\text{Clay—M}^{n+} + \text{NaCl} \longleftrightarrow \text{Clay—Na}^+ + \text{M—Cl}$$

where M is the metal ion present in the interlayer of the clay.

The previous reaction is reversible. Therefore, a higher concentration of the sodium chloride will favor the forward reaction. Because of this, a higher amount of sodium chloride was used (10% solution) for the *in situ* sodium activation of the bentonite clay.

During the addition of the amine hydrochloride in the aqueous solution of the bentonite clay, the following type of cation exchange reaction could have occurred with the amine hydrochloride and the sodium-activated clay:[33]

$$\text{Clay—Na}^+ + \text{ODAH}^+\text{Cl}^- \longleftrightarrow \text{Clay—ODAH}^+ + \text{NaCl}$$

Because the previous reaction is also a reversible reaction, the amount of amine hydrochloride is vital. A higher amount of amine cation with respect to the CEC equivalent of the clay was required to force the forward reaction. That is why amine content variation was used to determine the optimum dose.

In the A1 compound, bentonite clay was added from the master batch, in which the microscopic distribution of the clay particles had occurred. In the case of compound A2, the sodium montmorillonite fraction of the bentonite clay easily underwent a cation exchange reaction with the amine salt. This helped the SBR to penetrate into the interlayer of the

clay to some extent during mixing. The presence of less hydrated monovalent ions (K^+) and different types of multivalent metal ions in the bentonite clay reduced the cation exchange rate in compound A2. This was due to the fact that these ions could be capable of simultaneous interaction with anions on adjacent montmorillonite platelets, which made the intercalation more difficult for the amine.[40] Compound A3 contained the master batch in which the sodium chloride was added before the addition of the amine hydrochloride. The fraction of the bentonite clay that was not sodium montmorillonite underwent the cation exchange reaction and transformed into the sodium montmorillonite fraction. As a result, a maximum portion of the montmorillonite fraction of the bentonite clay was transformed into the sodium montmorillonite. Thus, in case of compound A3, the intercalation/exfoliation was easier and better. Thus, better properties were achieved because of the exfoliation/intercalation of the SBR in the sodium montmorillonite fraction of the bentonite clay in compound A3. The fact was also supported by the XRD data.

The previous mechanism explained the effect of the *in situ* sodium activation and organomodification.

CONCLUSIONS

This study represents an effective method of preparing a nanocomposite master batch. A substantial amount of increase in the physical properties were observed. *In situ* sodium activation of the unfractionated bentonite was carried out with the help of sodium chloride, and then, organomodification was carried out with the help of ODA. SBR latex and *in situ* sodium-activated, organomodified clay were mixed to prepare SBR/bentonite clay nanocomposites by a latex blending technique. FTIR study proved the presence of the ODA in the modified bentonite. The incorporation of this modified clay in the SBR matrix resulted in intercalation and/or exfoliation, as observed from the XRD and TEM results. The dispersion of the clay in the nanocomposites studied with the help of Si and Al mapping was better than the SBR/bentonite clay composites. The thermal stability of the nanocomposites showed improvement, as noticed from the peak decomposition temperature and peak decomposition rate. The DSC dynamic scans showed a positive shift in the elastomer T_g in the presence of the resol-modified nanoclay because of the confinement of rubber chains within the resol-modified bentonite layers, which restricted the segmental mobility of the SBR chains. The cure rates of the nanocomposites were higher because of the presence of amine. The mechanical properties of the nanocomposites showed tremendous improvement over the bentonite-clay-reinforced SBR composites. This method of co-coagulation of rubber latex and modified clay is very promising from the industrial viewpoint because of the low cost of the pristine clay, simplicity of the preparation technique, environmental friendliness, and good cost/performance ratio.

The authors thank the Hari Shankar Singhania Elastomer and Tyre Research Institute and the management of J. K. Tyre for their kind permission to publish this work.

References

1. Donnet, J. B. Compos Sci Technol 2003, 63, 1085.
2. Rubber Technology, 3rd ed.; Morton, M., Ed.; Chapman & Hall: London, 1995; Chapter 3, p 94.
3. Gorl, A.; Hunsche, U.; Muller, A.; Knaack, M.; Gobel, T. Kautsch Gummi Kunstst 1997, 50, 881.
4. Pramanik, M.; Srivastava, S. K.; Samantaray, B. K.; Bhowmick, A. K. J Appl Polym Sci 2003, 87, 2216.
5. Ganter, M.; Gronski, W.; Reichert, P.; Mulhaupt, R. Rubber Chem Technol 2001, 74, 221.
6. Ganter, M.; Gronski, W.; Semke, H.; Zilg, T.; Thomann, C.; Mulhaupt, R.; Kautsch Gummi Kunstst 2001, 54, 166.
7. Kojima, Y.; Fukumori, K.; Usuki, A.; Okada, A.; Kurauchi, T. J Mater Sci Lett 1993, 12, 889.
8. Vu, Y. T.; Mark, J. E.; Pham, L. H.; Engelhardt, M. J Appl Polym Sci 2001, 82, 1391.
9. Arroyo, M.; Lopez-Manchado, M. A.; Herrero, B. Polymer 2003, 44, 2447.
10. Lopez-Manchado, M. A.; Arroyo, M.; Herrero, B.; Biagiotti, J. J Appl Polym Sci 2003, 89, 1.
11. Teh, P. L.; Mohd Isak, Z. A.; Hashim, A. S.; Karger-Kocsis, J.; Ishiaku, U. S. J Appl Polym Sci 2004, 94, 2438.
12. Varghese, S.; Karger-Kocsis, J. J Appl Polym Sci 2004, 91, 813.
13. Teh, P. L.; Mohd Isak, Z. A.; Hashim, A. S.; Karger-Kocsis, J.; Ishiaku, U. S. J Appl Polym Sci 2006, 100, 1083.
14. Sengupta, R.; Sabharwal, S.; Bhowmick, A. K.; Chaki, T. K. Polym Degrad Stab 2006, 91, 1311.
15. Jia, Q.-X.; Wu, Y.-P.; Xu, Y.-L.; Mao, H.-H.; Zhang, L.-Q. Macromol Mater Eng 2006, 291, 218.
16. Theng, B. K. G. Formation and Properties of Clay–Polymer Complexes; Elsevier Scientific: Amsterdam, 1979.
17. Karger-Kocsis, J.; Wu, C.-M. Polym Eng Sci 2004, 44, 1083.
18. Varghese, S.; Karger-Kocsis, J. Polymer 2003, 44, 4921.
19. Wang, Y.; Zhang, H.; Wu, Y.; Yang, J.; Zhang, L. J Appl Polym Sci 2005, 96, 318.
20. Stephen, R.; Alex, R.; Cherian, T.; Varghese, S.; Joseph, K.; Thomas, S. J Appl Polym Sci 2006, 101, 2355.
21. Zhang, L.; Wang, Y.; Wang, Y.; Sui, Y.; Yu, D. J Appl Polym Sci 2000, 78, 1873.
22. Wang, Y.; Zhang, L.; Tang, C.; Yu, D. J Appl Polym Sci 2000, 78, 1879.
23. Zhang, H.; Wang, Y.; Wu, Y.; Zhang, L.; Yang, J. J Appl Polym Sci 2005, 97, 844.
24. Goodyear Tire & Rubber Co. U.S. Pat. 144401 A1 (2003).
25. Goodyear Tire & Rubber Co. U.S. Pat. 065266 A1 (2005).
26. Clay Containing Polymeric Nanocomposites; Utracki, L. A., Ed.; Rapra Technology: Shropshire, England, 2004; Vol. 1, Chapter 2.2, p 86.
27. Lietz, S.; Sandler, J. K. W.; Bosch, E.; Altstsdt, V. Kautsch Gummi Kunstst 2006, 59, 388.
28. Sadhu, S.; Bhowmick, A. K. Rubber Chem Technol 2005, 78, 321.

29. Sadhu, S.; Bhowmick, A. K. Rubber Chem Technol 2003, 76, 860.
30. Kawasumi, M.; Hasegawa, N.; Kato, M.; Usuki, A.; Okada, A. Macromolecules 1997, 30, 6333.
31. Gent, A. N.; Hartwell, J. A. Rubber Chem Technol 2003, 76, 517.
32. Wu, J.; Shen, Z.; Hu, D.; Huang, J.; Chen, N. Rubber Chem Technol 2000, 73, 19.
33. Clay Containing Polymeric Nanocomposites; Utracki, L. A., Ed.; Rapra Technology: Shropshire, England, 2004; Vol. 1, Chapter 2.2, p 88.
34. Lopez-Manchado, M. A.; Herrero, B.; Arroyo, M. Polym Int 2003, 52, 1070.
35. Kemp, W. Organic Spectroscopy, 3rd ed.; ELBS Macmillan: Hong Kong, 1994; p 66.
36. Mishra, J. K.; Kim, I.; Ha, C.-S.; Ryou, J.-H.; Kim, G.-H. Rubber Chem Technol 2005, 78, 42.
37. Science and Technology of Rubber, 1st ed.; Eirich, F. R., Ed.; Academic: New York, 1978; Chapter 7, p 299.
38. Rubber Technology, 1st ed.; Morton, M., Ed.; Chapman & Hall: London, 1995; Chapter 3, p 81.
39. Clay Containing Polymeric Nanocomposites; Utracki, L. A., Ed.; Rapra Technology: Shropshire, England, 2004; Vol. 1, Chapter 3.1, p 257.
40. Clay Containing Polymeric Nanocomposites; Utracki, L. A., Ed.; Rapra Technology: Shropshire, England, 2004; Vol. 1, Chapter 2.2, p 89.
41. Concise Inorganic Chemistry, 4th ed.; Lee, J. D., Ed.; Chapman & Hall: Singapore, 1993; Chapter 13, p 442.